Journal of Network Intelligence
Taiwan Ubiquitous Information
 ISSN 2414-8105
Volume **9**, Number **4**, November **2024**

Reactive Power Optimization of AC-DC Hybrid System Based on Improved Whale Algorithm

Xin-Yu Huang*

School of Electronic, Electrical Engineering and Physics
Fujian University of Technology
Fuzhou, 350118, P. R. China
544761865@qq.com

Quan Liang

School of Computer Science and Mathematics
Fujian University of Technology
Fuzhou, 350118, P. R. China
liangbruce@126.com

Xian-Fu Chen

School of Electronic, Electrical Engineering and Physics
Fujian University of Technology
Fuzhou, 350118, P. R. China
450047957@qq.com

Chuang-Tao Zhan

School of Electronic, Electrical Engineering and Physics
Fujian University of Technology
Fuzhou, 350118, P. R. China
1003797544@qq.com

*Corresponding author: Xin-Yu Huang
Received June 5, 2023, revised October 16, 2023, accepted January 18, 2024.

Abstract. *With the continuous construction of HVDC, it has gradually become distances and large capacity transmission, as well as one of the main technologies of regional power grid interconnection. The scale of AC-DC hybrid grid continues to grow, bringing new challenges to reactive power balance and voltage stability of power grid. An improved whale optimization algorithm is proposed to solve the reactive power optimization problem of AC-DC hybrid systems. By introducing local neighborhood search mechanism, adaptive threshold and adaptive inertia weight, the local search accuracy, global search ability and convergence speed of the algorithm are improved. The reactive power optimization model is established with the total network loss and node voltage offset as the objective function, and the solution steps are given. An IEEE 22-node system with DC transmission lines is used as an example to simulate the proposed algorithm, and compared with the traditional whale optimization algorithm and genetic algorithm, the results show that the proposed algorithm has good convergence and stability, and can obtain better reactive power optimization effect.*
Keywords: HVDC, AC-DC hybrid system, Reactive power optimization, Improved whale optimization algorithm

1. **Introduction.** Under the strategic objective of "carbon peak and carbon neutrality", cross-regional clean energy transmission will be strengthened. As an essential component of the smart power grid, the high voltage direct current (HVDC) technology is characterized by low line costs, flexible regulation, strong asynchronous networking ability, and its crucial role in achieving long-distance, large-capacity transmission of clean energy in our country [1]. With the completion and operation of a large number of HVDC power transmission projects, regional power grids have been connected through ultra-UHV AC-DC transmission lines. Our country has built the world's largest and highest voltage level AC-DC hybrid power grid to date [2]. In addition, effective management of reactive power balance and voltage stability is increasingly challenging in actual power grid operations. Therefore, the investigation of reactive power optimization has become an important strategy to enhance the economy and security of power grid operations.

Currently, both domestic and international research on reactive power optimization has mainly centered around single or multi-objective optimization of AC systems. However, the complexities of an AC-DC hybrid system require additional consideration of operational constraints associated with HVDC, making the optimization process more intricate. Traditional methods of optimization, such as interior point and dynamic programming, are susceptible to "dimensional disaster" [3]. Consequently, the introduction of intelligent optimization algorithms has ushered in new possibilities for the optimization of reactive power in AC-DC hybrid systems. In literature [4], genetic algorithm was initially utilized to handle the reactive power optimization problem encountered in AC-DC hybrid systems, resulting in faster convergence times when compared to traditional mathematical methods. In another related study [5], a fast non-dominated sorting genetic algorithm was developed with NSGA II strategy employed for multi-objective reactive power optimization. By directly addressing pareto optimal solutions without preliminary adjustments to the objective function weight value, this algorithm facilitates more efficient decision-making. A novel approach to reactive power optimization was presented in literature [6], which leverages the use of best point sets coupled with an improved quantum particle swarm optimization algorithm. This method has demonstrated superior performance in terms of global optimization search speed and stability. Literature [7] describes an improved backbone differential evolution algorithm which uses generalized reverse learning to initialize the population and adaptively adjusts the crossover probability, resulting in improved global optimization capabilities and greater robustness.

There are also many scholars who combine traditional algorithms with intelligent algorithms or combine multiple intelligent algorithms. Literature [8] combines interior point method with genetic algorithm, which can conveniently process discrete variables and has obvious directivity and good operation speed. Literature [9] proposes a simulated annealing genetic algorithm, which uses simulated annealing method as an individual replacement strategy in the process of genetic solution, realizes global optimization and has faster convergence speed. In literature [10], a fuzzy algorithm was applied to transform multi-objective optimization into single-objective optimization. The resulting model was then solved using biogeography algorithm to reduce the active power loss of the system and enhance the voltage quality at nodes. This approach was shown to be quite effective in achieving the optimization goals.

Despite the potential benefits of the aforementioned algorithms, they have been noted to suffer from certain limitations, such as low convergence accuracy, susceptibility to local optima, and operational complexities. To address these challenges, this paper proposes a new approach to reactive power optimization in AC-DC hybrid systems. Specifically, this study establishes a reactive power optimization model using total network loss and node voltage offset as the objective functions. This model is then solved using an improved

whale optimization algorithm (IWOA) built upon the traditional whale optimization algorithm (WOA). The IWOA algorithm introduces a local neighborhood search mechanism to improve the exploration capability of the algorithm, and a novel adaptive threshold is used to balance the global search and local development capabilities of the algorithm. Moreover, to enhance optimization accuracy and convergence speed, the algorithm incorporates an inertia weight derived from particle swarm optimization, as well as an adjusted position updating formula. To validate the efficacy and accuracy of IWOA, simulation analyses were carried out on an IEEE 22-node system with HVDC, and the optimization results were compared against those obtained using conventional and genetic algorithms.

2. AC-DC hybrid system model and power flow calculation.

2.1. AC-DC hybrid system model.

In the AC-DC hybrid system, the AC and DC systems are linked via a converter station, where the AC power is transformed into DC power using a converter transformer, converter valve group, flat-wave reactor, and filter circuit. This coupling process facilitates efficient power transmission between the two systems. To simplify the understanding of the AC-DC hybrid system model, Figure 1 illustrates the basic components and interconnections involved [11]. As shown in Figure 1, the various components of the AC-DC hybrid system are represented by different variables. U_{ac} and U_{dc} correspond to the respective AC and DC side voltages; P_{ac} and Q_{ac} denote the active and reactive power inputs from the AC side to the DC side; P_d and Q_d represent the active and reactive power inputs from the AC bus to the converter; P_{dc} and I_{dc} respectively represent DC power and DC current. I_b and I_s correspond to the DC power and DC current; k_t represents the transformer ratio of the converter. These variables play important roles in calculating the power flow of the AC-DC hybrid system.

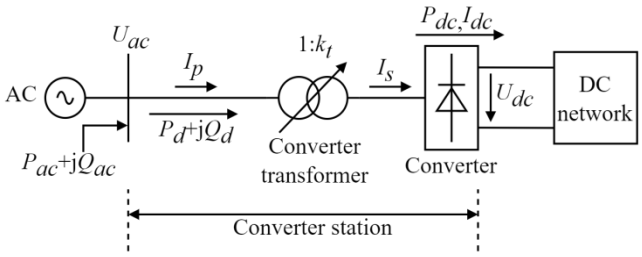

Figure 1. AC-DC hybrid system model

It is worth noting that the voltage drop caused by the reactance of the converter transformer is considered in the practical application of the AC-DC hybrid system. To ensure proper functionality of the system, the AC and DC voltages must satisfy certain requirements, which are outlined below:

$$U_{dc} = \frac{3\sqrt{2}}{\pi} n_b k_t U_{ac} \cos\theta - \frac{3}{\pi} n_b I_{dc} X_c \tag{1}$$

Where n_b represents the number of converter bridges; θ represents the control angle of the converter valve; X_c represents the equivalent reactance of the converter transformer.

Assuming that losses in the converter transformer can be neglected, the AC and DC voltages on both sides of the AC-DC hybrid system must satisfy the following conditions:

$$U_{dc} = \frac{3\sqrt{2}}{\pi} k_\gamma n_b k_t U_{ac} \cos\phi \tag{2}$$

Where k_γ is the coefficient introduced to consider the commutation overlap phenomenon, which is generally 0.995; φ represents the power factor angle of the converter.

During normal operation of the AC-DC hybrid system, the relationship between current and power can be described by the following set of equations:

$$\begin{cases} I_p = k_t I_s \\ I_s = k_\gamma k_t I_{dc} \\ n_b U_{ac} I_p \cos\varphi = U_{dc} I_{dc} \\ P_{dc} = U_{dc} I_{dc} \\ Q_d = P_d \tan\varphi \end{cases} \tag{3}$$

2.2. **Power flow calculation of AC-DC hybrid system.** The calculation of power flow within an AC-DC hybrid system is fundamental to optimizing reactive power, and can be solved using various methods, including the unified iteration method and the alternating iteration method [**?**]. The unified iteration method employs a Newton method in polar coordinates to perform a unified iterative solution for all variables within the AC and DC systems. However, this approach can be complex and computationally intensive. Alternatively, the alternating iteration method simplifies the unified iteration method by separately solving the DC and AC systems. Specifically, when calculating the power flow of the DC system, the load power of the DC system is provided for the AC system. Conversely, when calculating the power flow of the AC network, the balance node voltage value is provided for the DC network. In this paper, the power flow distribution of the AC-DC hybrid system is calculated using the idea of alternating iteration method and push-back method.

Figure 2 illustrates the flow of the power flow calculation process. Initially, the original parameters are input and the initial voltage values of all unknown nodes are established. Subsequently, the AC node connected to the primary side of the converter is selected as the balance node for power flow calculation of the DC system. The voltage and power of each node in the DC system are calculated using the push-back method, and the maximum voltage error ΔV_{dc} at each node is obtained. The value ΔV_{dc} is then checked to determine if it meets the required degree of convergence accuracy ϵ. If $|\Delta V_{dc}| < \epsilon$, the load power for the DC system, equivalent to the AC node of the converter, is calculated directly, followed by the computation of the power flow of the AC system using the push-back substitution method. If $|\Delta V_{dc}| > \epsilon$, the power flow of the DC system and ΔV_{dc} are recalculated until the requirements are met. Similarly, the maximum voltage error ΔV_{ac} for each node in the AC system can be evaluated until the voltage of both the AC and DC systems meet the required convergence accuracy levels. Once this occurs, the iterative process can be terminated and the results can be output.

2.3. **Reactive power optimization model of AC-DC hybrid system.**

2.3.1. *Objective function.* The converter in an AC-DC hybrid system typically consumes a significant amount of reactive power during operation, which can vary depending on the operating mode and impact system voltage stability. To mitigate this, the generator terminal voltage, transformer ratio, and reactive power compensation device switch quantity can be adjusted to control system voltage and reduce network losses. In this paper, the objective function F is defined as the total network loss and node voltage offset of the AC-DC hybrid system, and is expressed as follows:

$$\min F = \omega_1 (P_{\text{ac,Loss}} + P_{\text{dc,Loss}}) + \omega_2 f_{\Delta V} \tag{4}$$

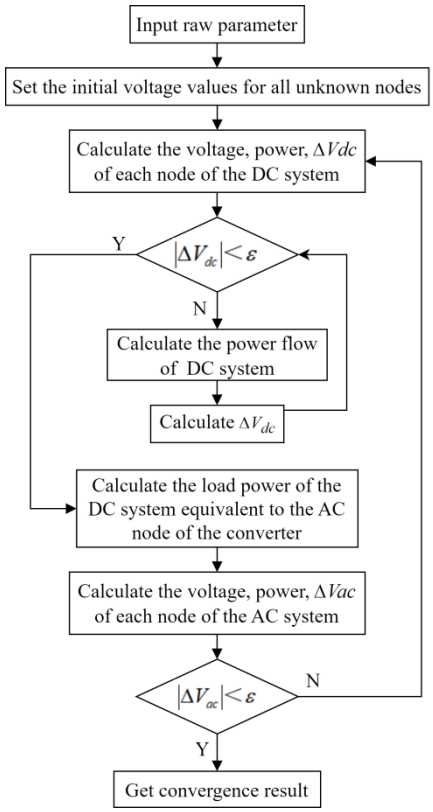

Figure 2. Power flow calculation process

$$P_{\text{ac,Loss}} = \sum_{k=1}^{n_1} G_{(i,j)} \left(U_i^2 + U_j^2 - 2U_i U_j \cos\theta_{ij}\right) \tag{5}$$

$$P_{\text{dc,Loss}} = \sum_{k=1}^{n_2} I_{dk}^2 R_{dk} \tag{6}$$

$$f_{\Delta U} = \sum_{i \in N_{PQ}} \left| \frac{U_i^b - U_i}{U_i^{\max} - U_i^{\min}} \right| \tag{7}$$

Where $P_{\text{ac,Loss}}$ and $P_{\text{dc,Loss}}$ denote the network loss in the AC and DC systems, respectively; $f_{\Delta V}$ represents the voltage offset; The weighting coefficients ω_1 and ω_2 are used to balance the impact of network loss and voltage offset on the objective function; $G_{(i,j)}$ is expressed as the conductance on the k branch of the AC system; U_i and U_j represent the voltage amplitude of nodes i and j; θ_{ij} represents the phase angle difference between nodes i and j; I_{dk} and R_{dk} respectively represent the current and resistance on the k branch of the DC system; n_1 and n_2 respectively represent the number of branches of AC and DC systems; N_{PQ} represents the set of PQ busbars; U_i^b, $U_i^{\max}$, and $U_i^{\min}$ represent the voltage reference value, voltage upper limit, and voltage lower limit of node i, respectively.

2.3.2. *Equality constraint.* The Equation constraint pertains to the power balance Equation of the power system with power flow constraint, and is expressed as follows [13]:

$$\begin{cases} P_{Gi} - P_{Li} - \mu P_{Di} = U_i \sum_{j=1}^{N} U_j \left(G_{ij}\cos\theta_{ij} + B_{ij}\sin\theta_{ij}\right) \\ Q_{Gi} + Q_{Ci} - Q_{Li} - \mu Q_{Di} = U_i \sum_{j=1}^{N} U_j \left(G_{ij}\sin\theta_{ij} - B_{ij}\cos\theta_{ij}\right) \end{cases} \tag{8}$$

Where P_{Gi} and Q_{Gi} respectively represent the active power and reactive power output of the AC system generator node; P_{Li} and Q_{Li} respectively represent the active power and reactive power load of node i; P_{Di} and Q_{Di} respectively represent the active power and reactive power transmitted by node i to the connected converter; Q_{Ci} represents the reactive power compensation capacity of the node; N represents the total number of system nodes; G_{ij} and B_{ij} respectively represent the conductance and susceptance between nodes i and j; μ is a parameter representing the direction of active power flowing into or out of the converter. Specifically, when the node is the rectifier side, $\mu = 1$; when the node is the inverter side, $\mu = -1$.

2.3.3. *Inequality constraint.* The inequality constraints comprise the upper and lower limits of control variables and state variables. When the system runs normally, each variable must be limited in a reasonable range. The control variables consist of the generator node terminal voltage, on-load regulator transformer ratio, reactive power compensation node compensation capacity, as well as the control voltage, control current, control power, and control angle of the converter in the DC system. On the other hand, the state variables comprise the reactive power output of the generator node, voltage of the load node, branch reactive power flow, and converter transformer ratio [14].

The constraints on the control variables can be represented as:

$$\begin{cases} U_{g_{\min}} \le U_{gi} \le U_{g_{\max}} \\ T_{\min} \le T_i \le T_{\max} \\ Q_{ci_{\min}} \le Q_{ci} \le Q_{ci_{\max}} \\ U_{d_{\min}} \le U_{di} \le U_{d_{\max}} \\ I_{d_{\min}} \le I_{di} \le I_{d_{\max}} \\ P_{d_{\min}} \le P_{di} \le P_{d_{\max}} \\ \cos\theta_{d_{\min}} \le \cos\theta_{di} \le \cos\theta_{d_{\max}} \end{cases} \tag{9}$$

Where U_{gi} is the terminal voltage of generator i; T_i is the ratio of on-load regulating transformer i; Q_{ci} is the compensation capacity of capacitor i; U_{di}, I_{di}, P_{di} and θ_{di} are respectively the voltage, current, power and control angle of the i-th converter in the DC system.

State variable constraints can be expressed as:

$$\begin{cases} Q_{g_{\min}} \le Q_{gi} \le Q_{g_{\max}} \\ U_{i_{\min}} \le U_i \le U_{i_{\max}} \\ Q_{zi_{\min}} \le Q_{zi} \le Q_{zi_{\max}} \\ K_{i_{\min}} \le K_i \le K_{i_{\max}} \end{cases} \tag{10}$$

Where Q_{gi} is the reactive power output of generator i; U_i is the voltage of load node i; Q_{zi} is the reactive power of branch i; K_i is the ratio of the i-th converter transformer.

3. **The improved whale optimization algorithm was used to solve the model.**

3.1. **Whale optimization algorithm.** Based on the distinctive bubble net predation strategy of humpback whales, the WOA algorithm is a biomimetic swarm intelligence approach that can be broadly divided into three distinct phases: surround the prey, bubble net attack, and search for prey [15, **?**, 16, 17].

3.1.1. *Surround the prey.* During the hunting process, the humpback whale pod must communicate to coordinate their movements and approach the nearest individual to the prey, which represents the current local optimal solution. The nearby whale then randomly attempts to approach the prey, driving the entire group gradually closer to and surrounding their target. This stage can be mathematically modeled as follows:

$$\overrightarrow{D} = \left| \overrightarrow{C} \cdot \overrightarrow{X^*}(t) - \overrightarrow{X}(t) \right| \tag{11}$$

$$\overrightarrow{X}(t+1) = \overrightarrow{X^*}(t) - \overrightarrow{A} \cdot \overrightarrow{D} \tag{12}$$

Where t denotes the current iteration number; $\overrightarrow{D}$ is the distance between an individual whale and its prey. $\overrightarrow{X}(t)$ is the position vector of the individual whale; $\overrightarrow{X^*}(t)$ represents the position vector of the current optimal solution; $\overrightarrow{A}$ and $\overrightarrow{C}$ are coefficient vectors written as follows:

$$\overrightarrow{A} = 2\overrightarrow{a} \cdot \overrightarrow{r} - \overrightarrow{a} \tag{13}$$

$$\overrightarrow{C} = 2 \cdot \overrightarrow{r} \tag{14}$$

$$\overrightarrow{a} = 2 - \frac{2t}{T_{\max}} \tag{15}$$

Where $\overrightarrow{a}$ is the control parameter that decreases linearly from 2 to 0 with an increasing number of iterations. $\overrightarrow{r}$ is the random vector with values between $[0, 1]$; $T_{\max}$ is the maximum number of iterations.

3.1.2. *Bubble net attack.* A key feature of the bubble net predation method is moving in a spiral path while constricting the encircling circle. WOA adopts two strategies of shrink encircling and spiral update position to simulate. In the process of linear decline of $\overrightarrow{a}$, the value range of $\overrightarrow{A}$ is $[-\overrightarrow{a}, \overrightarrow{a}]$. When $\overrightarrow{A}$ is the random value in $[-1, 1]$, the whale after position update is located at any position between the original position and the prey, so that every whale is close to the prey. The mathematical formulation of this stage is expressed as follows:

$$\overrightarrow{D}' = \left| \overrightarrow{X^*}(t) - \overrightarrow{X}(t) \right| \tag{16}$$

$$\overrightarrow{X}(t+1) = \overrightarrow{D}' e^{bl} \cos(2\pi l) + \overrightarrow{X^*}(t) \tag{17}$$

Where $\overrightarrow{D}'$ denotes the distance between an individual whale and its prey in the t-th generation; b is the constant that defines the shape of the logarithmic spiral and is set to 1; l is the random number between $[-1, 1]$.

When approaching prey, contraction encircle and spiral update position are carried out simultaneously. In order to simulate this hunting process, a probability threshold is introduced to judge which way individual whales perform. The value of p is a random number between $[0, 1]$, and its mathematical representation is as follows:

$$\overrightarrow{X}(t+1) = \begin{cases} \overrightarrow{X^*}(t) - \overrightarrow{A} \cdot \overrightarrow{D} & p < 0.5 \\ \overrightarrow{D}' e^{bl} \cos(2\pi l) + \overrightarrow{X^*}(t) & p \geq 0.5 \end{cases} \tag{18}$$

3.1.3. *Search for prey.* In contrast to the contract-encircle approach, when $|\overrightarrow{A}| > 1$, the whale group no longer updates its position based on the prey. Instead, the group randomly selects a reference whale to replace the role of prey, which allows for greater exploration of the search space and the possibility of obtaining the global optimal solution. The mathematical representation of this stage is as follows:

$$\overrightarrow{D}_{\text{rand}} = \left| \overrightarrow{C} \cdot \overrightarrow{X}_{\text{rand}} - \overrightarrow{X}(t) \right| \tag{19}$$

$$\overrightarrow{X}(t+1) = \overrightarrow{X}_{\text{rand}} - \overrightarrow{A} \cdot \overrightarrow{D}_{\text{rand}} \tag{20}$$

Where $\overrightarrow{X}_{\text{rand}}$ is the position vector of the individual whale; $\overrightarrow{D}_{\text{rand}}$ is the distance between an individual whale and its prey.

3.2. **Improved whale optimization algorithm.**

3.2.1. *Local neighborhood search.* To enhance the local search abilities of the WOA algorithm, a local neighborhood search mechanism is integrated. For each current solution X_t^i, a local population of N solutions is generated by centering on X_t^i. The population is then surrounded by Equation (21) in order to obtain the local optimal solution X_t^i. Then, the local population is iterated T times by Equation (22), and the new local population and the optimal solution are obtained. Finally, the current solution X_t^i is replaced with the optimal solution, and then the follow-up search is carried out. The mechanism is expressed as follows:

$$X_{ij}^l = \frac{1}{2}(ub - lb)(r_a - r_b)a + X_i^l \tag{21}$$

$$X_i^{t+1} = \begin{cases} r_{sc} \sin(r_s) \cdot X_i^t & r_p < 0.5 \\ r_{sc} \cos(r_s) \cdot X_i^t & r_p \geq 0.5 \end{cases} \tag{22}$$

Where X_{ij}^l is the j-th solution in the local population; ub and lb refer to the upper and lower limits, respectively, of the solution space. r_a and r_b are random numbers between $[0, 1]$. a is the global search range attenuation factor, and the calculation formula is the same as Equation (15). r_{sc} is an adaptive random quantity whose value decreases linearly from 4 to 0; r_s and r_p are random variables with the value ranges of $[0, 2\pi]$ and $[0, 1]$ respectively.

3.2.2. *Adaptive probability threshold.* The WOA algorithm employs a fixed probability threshold of 0.5 to select a hunting strategy by comparing a random number p with it. However, as the number of iterations increases, the algorithm is susceptible to getting stuck in local optima. To circumvent this issue, this paper suggests using an adaptive probability threshold p', which balances the algorithm's global search and local exploitation capabilities. This threshold is calculated using the following expression:

$$p' = 1 - \log_{10}\left(1 + \frac{9t}{T_{max}}\right) \tag{23}$$

Early in the iteration, the adaptive threshold is large, and the whales adopt the shrinking and encircling strategy with high probability. In the late iteration period, the adaptive threshold is small, and the whales adopt the spiral updating strategy with high probability. IWOA synchronously optimizes the two methods of the traditional algorithm to first shrink and surround and then spiral update the position. With the adaptive probability threshold p' being updated constantly, the algorithm rapidly approaches the optimal solution, thereby boosting its convergence speed.

3.2.3. *Adaptive inertia weight.* WOA carries out local search through Equations (12) and (17), and can only approach the local optimal solution, but cannot carry out better local optimization. As there is no corresponding weight adjustment, individual whales will stay near the theoretical position, which is prone to premature convergence. This paper proposes an adaptive inertia weight strategy to tackle this issue. The inertia weight, which is introduced in the particle swarm optimization algorithm, adjusts the position update formula of the algorithm. The relevant expression is as follows:

$$\omega = (\omega_{start} - \omega_{end}) \cdot 0.8 \times \left[1 - \left(\frac{t}{T_{max}}\right)^k\right] + \omega_{end} \tag{24}$$

Where ω is the weight at the beginning of iteration, and its value is 0.9; ω_{end} is the weight at the end of iteration, and the value is 0.4. The control factor k, regulates the smoothness of the curve and has a value of 0.6.

With a high initial weight, the algorithm exhibits strong global search capabilities, while a low weight value towards the end of the iteration leads to fine-grained search near the optimal solution to prevent local optima. The optimized mathematical model is expressed as:

$$X(t+1) = \begin{cases} \omega \cdot \vec{X}^*(t) - \vec{A} \cdot \vec{D} & \text{if } |\vec{A}| < 1,\ p < p' \\ \omega \cdot \vec{X}_{rand} - \vec{A} \cdot \vec{D}_{rand} & \text{if } |\vec{A}| \geq 1,\ p < p' \\ D' \cdot e^{bl} \cdot \cos(2\pi l) + \omega \cdot \vec{X}^*(t) & \text{if } p \geq p' \end{cases} \tag{25}$$

3.3. **Reactive power optimization flow of AC-DC hybrid system.** Figure 3 illustrates the reactive power optimization process using the IWOA algorithm. To begin, the system and algorithm parameters are input to generate an initial population randomly. Next, power flow calculations are performed, and the fitness function is employed to determine the fitness of each individual in the initial population. Then the local neighborhood search is carried out to obtain the local optimal solution initially. Parameters A, C, p', and ω are updated successively according to the algorithm steps. Then, the corresponding size relationship of p' and $|A|$ is judged by Formula (25), and different formulas are adopted to update individual positions. Upon the attainment of the maximum iteration number $T_{\max}$ by the current iteration count t, the optimal solution is outputted as the convergence condition is fulfilled.

4. Example analysis.

4.1. **Example data.** This paper utilizes the IEEE 22-node system from literature [**?**] as a case study for reactive power optimization analysis, and its topology is illustrated in Figure 4. The AC-DC hybrid system with DC transmission lines is formed by replacing the original 11-12 AC branches with HVDC and eliminating the shunt reactance in these two nodes.

In this system, node 1 is the equilibrium node, nodes 3 and 6 are PV nodes, nodes 11 and 12 are DC nodes, and the rest nodes are PQ nodes. DC node 11 serves as the rectifier side, and DC node 12 functions as the inverter side. A compensator is installed on the converter station to provide reactive power consumed by its own commutation. For the rectifier side, a control mode of constant power and hysteresis triggering angle is adopted, while the inverter side is controlled by a constant voltage and advance arc quenching angle mode. The parameters for the HVDC system are listed in Table 1, in which control mode A denotes the fixed power and voltage parameters for the rectifier and inverter sides, while control mode B depicts the fixed lag triggering angle and advance arc quenching angle for rectifier and inverter sides, respectively.

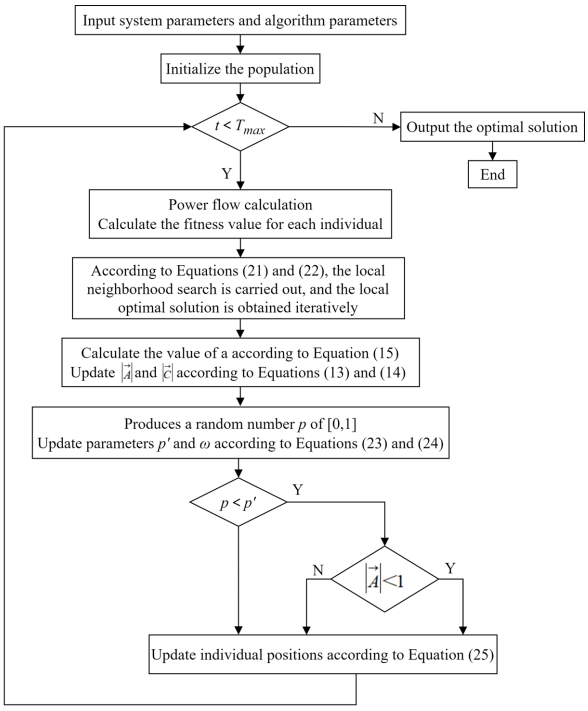

Figure 3. IWOA reactive power optimization process

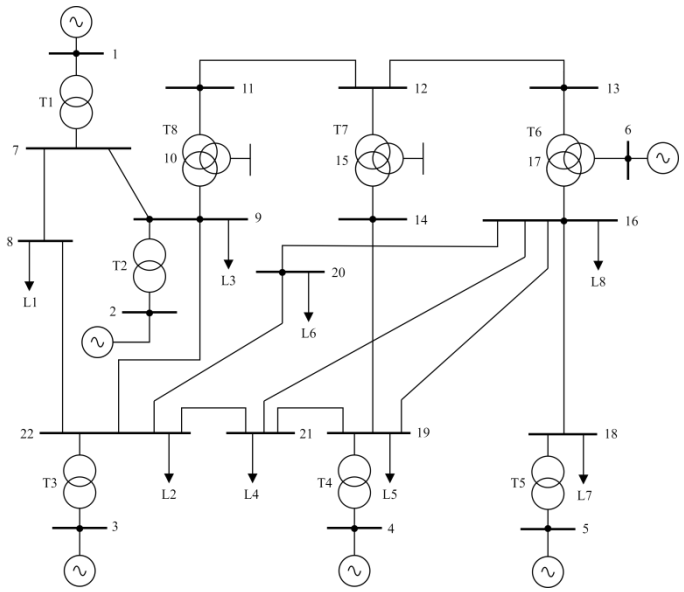

Figure 4. IEEE 22 node topology

The power flow distribution of the AC-DC hybrid system is computed with a convergence accuracy ε of 10^{-5}, and the calculation results are presented in Table 2. By utilizing the proposed power flow calculation method, the number of iterations remains the same as the alternating iteration method. However, this approach reduces the calculation load of power flow while ensuring convergence, leading to a slightly faster solving speed.

The limiting values of each control variable in this paper are shown in Table 3. The ratio of on-load regulating transformer is used as discrete control variable, the gear position is divided into 16 gears, and the adjustment step is 0.0125. The other variables are used as continuous control variables, and the mode of shunt capacitor is adopted for reactive power

Table 1. HVDC parameter per unit value

Subordinate part	**Rectifier**	**Inverter**
Node	11	12
Commutation reactance	0.0130	0.0130
Voltage	1.0000	0.9384
Current	1.5000	1.5000
Power factor angle	0.4510	0.4510
Transformer ratio	1.1167	1.0479
Control mode A	1.5000 (Power)	0.9384 (Voltage)
Control mode B	0.4202 (Hysteresis trigger angle)	0.4175 (Advance arc Angle)

Table 2. Power flow distribution of IEEE 22-node AC-DC hybrid system

Node	**Voltage amplitude/p.u.**	**Voltage phase Angle/°**	**Active power/p.u.**	**Reactive power/p.u.**
1	1.0000	0.0000	6.6492	1.9803
2	0.9874	-0.2356	6.0000	3.2000
3	1.0000	-0.7978	3.1000	4.1390
4	1.0189	-0.8956	1.6000	0.7000
5	1.0390	-0.9478	4.3000	3.3400
6	1.0000	-1.1141	-0.0100	1.0479
7	1.0242	-0.1024	0.0000	-0.3112
8	0.9743	-0.3912	-2.8700	-1.4400
9	0.9960	-0.3784	-3.7600	-2.2100
10	0.9933	-0.3754	0.0000	0.0000
11	1.0186	-0.4021	0.0000	0.0000
12	1.0144	-1.0318	0.0000	-0.5000
13	0.9862	-1.0893	0.0000	0.0000
14	1.0041	-1.0172	0.0000	-0.5000
15	1.0028	-1.0154	0.0000	0.0000
16	0.9879	-1.1162	-5.0000	-2.9000
17	0.9647	-1.1137	0.0000	-0.4425
18	0.9781	-1.1152	-4.3000	-2.6000
19	1.0046	-0.9983	-0.8640	-0.6620
20	0.9980	-1.0190	-0.7190	-0.4740
21	1.0061	-0.9695	-0.7000	-0.5000
22	1.0444	-0.8383	-2.2650	-1.6900

compensation devices. In this example, the reference power of the system is 100MV·A, the voltage lower limit of all load nodes is 0.95p.u., the voltage upper limit of PQ node and balance node is 1.05p.u., and the voltage upper limit of PV node is 1.1p.u. This paper increases the node load to 1.2 times and obtains the voltage distribution curve of the IEEE 22-node system, as demonstrated in Figure 5. The voltage of node 18 falls below the safe lower limit, the voltage level of node 17 approaches the lower limit, and several nodes exhibit a voltage level lower than the average level. Therefore, to regulate the voltage level, reactive power compensation is required.

4.2. **Analysis of reactive power optimization results.** To demonstrate the efficacy of the IWOA algorithm, this paper conducts a comparative analysis of the reactive power

Table 3. Control variable qualification value

Control variable	Upper limit	Lower limit	Control variable	Upper limit	Lower limit
Generator terminal voltage	1.1	0.9	Load regulating transformer ratio	1.1	0.9
Reactive power compensation capacity	0.5	0	DC voltage	1.1	0.9
DC current	1	0.1	DC power	0.5	0
Trigger angle	18°	8°	Arc angle	28°	18°

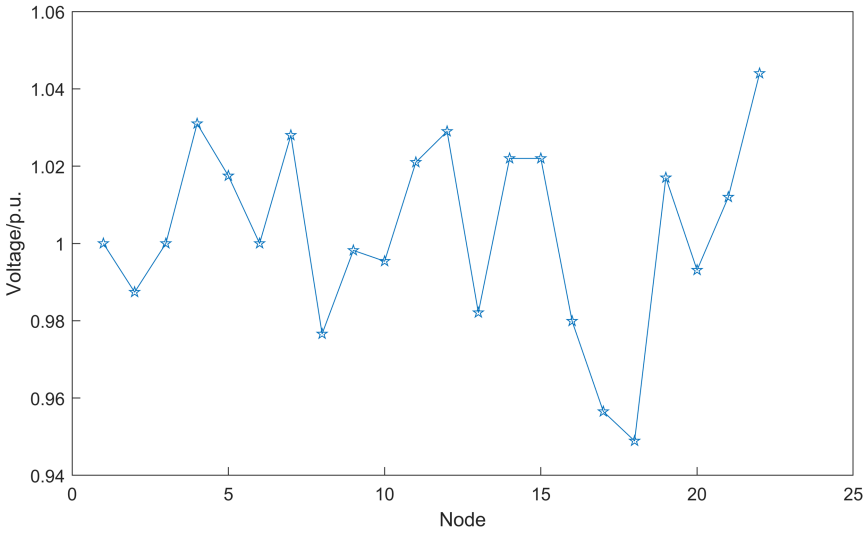

Figure 5. IEEE 22 Voltage distribution curve of each node

optimization results obtained by IWOA, WOA, and GA algorithms. The population size and iteration number are fixed at 20 and 100 respectively. Figure 6 illustrates the evolution curve of the fitness function for these three algorithms.

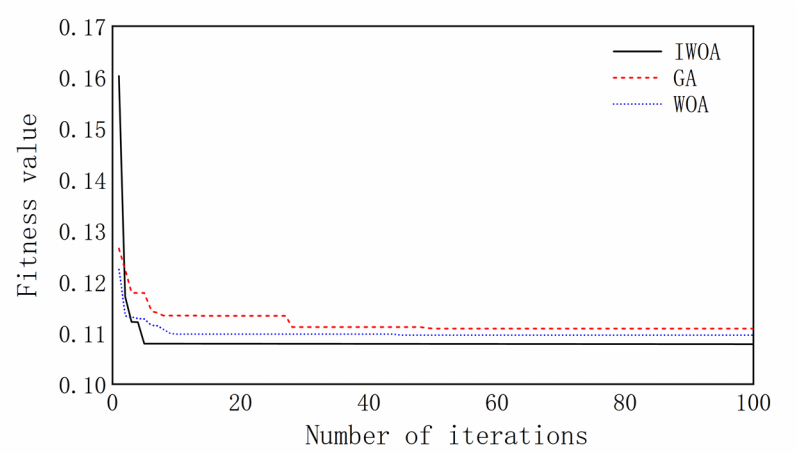

Figure 6. Convergence curves of different algorithms.

The results suggest that the GA algorithm reaches local optimization early in the iterative process, while the WOA algorithm falls into local optimization after about 45 iterations. On the contrary, the IWOA algorithm achieves the optimal solution around the 6th iteration, demonstrating better convergence ability and speed compared to the other two algorithms. It can obtain better solutions with less computational effort while avoiding local optimization and achieving global optimization more effectively. Table 4 presents the reactive power optimization results obtained in this study.

Table 4. Reactive power optimization results and comparison

Control quantity	**Upper limit**	**Lower limit**	**Optimization result**		
			IWOA	**WOA**	**GA**
U_{g1}	1.1	0.9	1.0600	1.0600	1.0600
U_{g2}	1.1	0.9	0.9894	0.9881	0.9875
U_{g3}	1.1	0.9	1.0185	1.0170	1.0178
U_{g4}	1.1	0.9	1.0313	1.0296	1.0205
U_{g5}	1.1	0.9	1.0246	1.0185	1.0159
U_{g6}	1.1	0.9	1.0720	1.0720	1.0715
T_1	1.1	0.9	1.0500	1.0375	1.0375
T_2	1.1	0.9	0.9875	1.0375	1.0125
T_3	1.1	0.9	1.1000	1.0750	1.0750
T_4	1.1	0.9	1.0250	1.0250	1.0250
T_5	1.1	0.9	1.0500	1.0500	1.0625
T_6	1.1	0.9	1.0375	1.0250	1.0250
T_7	1.1	0.9	1.1000	1.0000	1.0000
T_8	1.1	0.9	1.0375	1.0500	1.0375
Q_8	0.5	0	0.0284	0.0086	0.0061
Q_{13}	0.5	0	0.3498	0.3000	0.3098
Q_{16}	0.5	0	0.2866	0.2810	0.2294
Q_{17}	0.5	0	0.3129	0.3066	0.1265
Q_{18}	0.5	0	0.4011	0.3958	0.3333
P_{11}	0.2	0	0.0618	0.0618	0.0618
U_{12}	1.1	0.9	1.0298	1.0275	1.0275
K_{11}	1.1	0.9	1.0375	1.0000	1.0000
K_{12}	1.1	0.9	1.0000	1.0300	1.0300

In the table, $U_{g1} \sim U_{g6}$ is the voltage of each generator node; $T_1 \sim T_8$ is the transformer ratio; $Q_{c8}, Q_{c13}, Q_{c16}, Q_{c17}, Q_{c18}$ is the reactive power compensation amount of each node; P_{11} and U_{12} are the power of rectifier stations at 11 nodes and the voltage of inverter stations at 12 nodes respectively. K_{11} and K_{12} are the ratio of the rectifier station and the inverter station.

Figure 7 displays the optimized voltage distribution curve of the IEEE 22-node system. Prior to reactive power optimization, nodes 8, 17, and 18 had the lowest voltage levels in the system. Following reactive power optimization, the voltage of node 18 is restored to within the acceptable range, and the voltage levels of other nodes are also enhanced to some extent.

The results of the target values optimized by the three algorithms are shown in Table 5. Based on the simulation results discussed above, it can be concluded that the proposed IWOA algorithm effectively reduces system network losses and node voltage deviations through reactive power optimization. The optimization results demonstrate

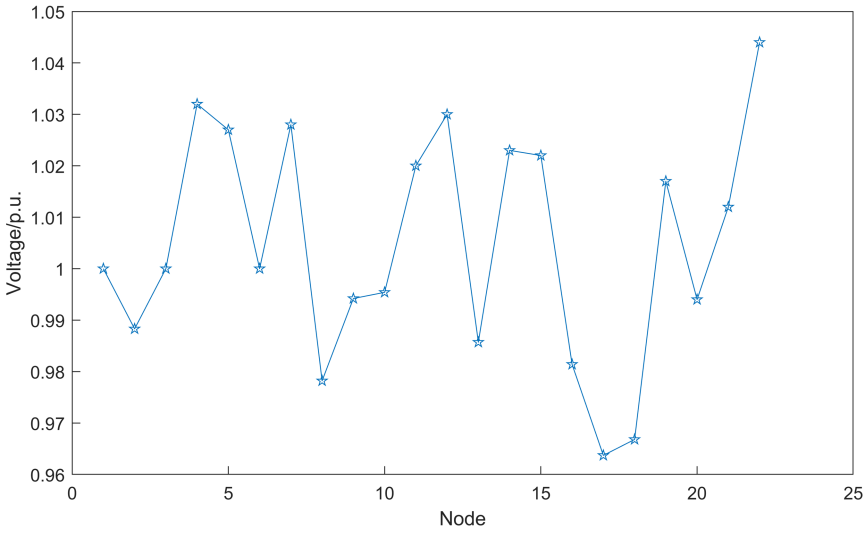

Figure 7. Voltage distribution curves of each node after optimization

Table 5. Each target value and comparison

Target value	**Initial result**	**Optimization result**		
		IWOA	**WOA**	**GA**
Total network loss	1.2143	1.2014	1.2037	1.2075
Node voltage offset	0.1185	0.1076	0.1109	0.1116
Objective function F	—	0.1075	0.1108	0.1116

superior improvement in voltage quality and reduction of network losses compared to the WOA and GA algorithms. Furthermore, the capacity of each compensation device is within a suitable range.

5. **Conclusion.** This study proposes an improved whale optimization algorithm to address the problem of reactive power optimization in AC-DC hybrid systems. First, the model of the AC-DC hybrid system is presented, and the system's power flow distribution is calculated using the alternating iteration method and backward-forward substitution method. Second, an objective function for the reactive power optimization model is established, taking into consideration the total network loss and node voltage offset. Third, the proposed improved whale optimization algorithm is applied to optimize the model. The algorithm incorporates a local neighborhood search mechanism, adaptive threshold, and adaptive inertia weight to enhance the reactive power optimization process. Finally, simulations are performed on an IEEE 22-node system with HVDC, and the effectiveness of the proposed algorithm is analyzed and compared with traditional algorithms. The results suggest that the proposed algorithm outperforms traditional algorithms in terms of improving voltage quality and reducing network losses while maintaining reasonable capacity of each compensation device.

(1) On the premise of ensuring convergence, the established power flow model reduces the calculation amount.

(2) The proposed algorithm can realize global optimization, has good convergence ability and convergence speed, and has better optimization effect.

(3) Although the algorithm in this paper realizes global optimization through optimization, it is not considered to be applied to the actual complex system. If can combine

with other intelligent algorithm, can make further improvement to the performance of the algorithm.

Acknowledgment. This work is partially supported by the Science and Technology Program of Fujian Province of China (No. 2020H0021).

REFERENCES

[1] Z.-Y. Lei, L.-S. Hao, J.-S. Dai, L. Zhang, X. Wang, C.-Y. Cui, J.-C. Qi, and X.-J. Tang, "A review of fault location methods in HVDC transmission lines," *Power System Protection and Control*, vol. 50, no. 11, pp. 178-187, 2022.

[2] X.-Z. Dong, Y. Tang, G.-Q. Bu, C. Shen, G.-B. Song, Z.-P. Wang, D.-Q. Gan, J.-X. Hou, B. Wang, B. Zhao, and S.-X. Shi, "Confronting problem and challenge of large scale AC-DC hybrid power grid operation," *Proceedings of the CSEE*, vol. 39, no. 11, pp. 3107-3119, 2019.

[3] K.-W. Wang and D.-Y. Zhang, "Review of reactive power optimization algorithms for power systems," *Electrical Measurement & Instrumentation*, vol. 53, no. 10, pp. 73-19+98, 2016.

[4] U. Kilic, K. Ayan, and U. Arifoglu, "Optimizing reactive power flow of HVDC systems using genetic algorithm," *International Journal of Electrical Power & Energy Systems*, vol. 55, pp. 1-12, 2014.

[5] L. Ren and J. Zhang, "Reactive power optimization of AC and DC system based on improved genetic algorithm," in *Journal of Physics: Conference Series*. IOP, 2020, pp. 052028.

[6] H.-K. Li, Z.-J. Xie, Z.-F. Chen, and W.-J. Zhang, "Reactive power optimization of AC-DC power system based on the good-point set quantum particle swarm algorithm," *Journal of Electric Power Science and Technology*, vol. 31, no. 03, pp. 95-102, 2016.

[7] T. Zhang, R.-J. Zhu, and D.-Z. ZhaXi, "Reactive power optimization of hybrid AC-DC system based on improved bare-bones differential evolution algorithm," *Electrical Measurement & Instrumentation*, vol. 58, no. 05, pp. 78-85, 2021.

[8] P. Jiang and L. Liang, "Reactive power optimization of hybrid AC/HVDC power system combining interior point algorithm and genetic algorithm," *High Voltage Engineering*, vol. 41, no. 03, pp. 724-729, 2015.

[9] J.-H. Huang, W.-Y. Wang, H.-Q. Wang, and H.-K. Li, "Study of hybrid genetic algorithm and annealing algorithm on reactive power," *Power System Protection and Control*, vol. 44, no. 10, pp. 37-43, 2016.

[10] W.-X. Liu, L.-H. Xing, C.-H. Ma, and W.-B. Li, "Multi-objective reactive power optimization of hybrid AC-DC power system considering power system uncertainty," in *Journal of Physics: Conference Series*. IOP, 2019, pp. 02239.

[11] X.-F. Wang, *Analysis of modern power systems*, Beijing: Science Press, 2003.

[12] X.-C. Lv, X.-X. Li, C. Fu, H. Li, Z.-A. Zeng, J.-Y. Guo, and Y.-P. Fan, "Power flow decoupling algorithm for hybrid AC-DC system based on alternating iteration method," *Engineering Journal of Wuhan University*, vol. 55, no. 12, pp. 1263-1270, 2022.

[13] H. Farahmand, M. Rashidinejad, A. Mousavi, A.A. Gharaveisi, M.R. Irving, and G.A. Taylor, "Hybrid mutation particle swarm optimisation method for available transfer capability enhancement," *International Journal of Electrical Power & Energy Systems*, vol. 42, no. 1, pp. 240-249, 2012.

[14] X.-M. Wu and H. Wang, "Reactive power optimization of AC-DC system on NSGA II," *Journal of Xi'an Shiyou University (Natural Science Edition)*, vol. 34, no. 05, pp. 122-126, 2019.

[15] D.-G. Xu, Z.-Q. Wang, Y.-X. Guo, and K.-J. Xing, "Review of whale optimization algorithm," *Application Research of Computers*, vol. 40, no. 02, pp. 328-336, 2023.

[16] L. Liu and Q. He, "Improved whale optimization algorithm for solving function optimization problems," *Application Research of Computers*, vol. 37, no. 04, pp. 1004-1009, 2020.

[17] Z.-Q. Wu and Y.-M. Mou, "An improved whale optimization algorithm," *Application Research of Computers*, vol. 37, no. 12, pp. 3618-3621, 2020.

[18] T.-Y. Wu, H.-N. Li, and S.-C. Chu, "CPPE: An Improved Phasmatodea Population Evolution Algorithm with Chaotic Maps," *Mathematics*, vol. 11, no. 9, pp. 1977, 2023.

[19] S.-X. Zhou, *Voltage stability and control of power systems*, Beijing: China Electric Power Press, 2004.